CT-FEA of Inhomogeneous Lumbar with Different Loadings of the Spinal Cage

Muhammad Shahruddin Azmi[1], Munirah Mohamad Izham[2], Muhammad Hilmi Jalil[1]*, Muhammad Hazli Mazlan[3]

[1]Faculty of Mechanical and Automotive Engineering Technology, Universiti Malaysia Pahang Al-Sultan Abdullah, Pekan, Pahang, Malaysia
[2]College of Engineering, Universiti Malaysia Pahang Al-Sultan Abdullah, 26600 Pekan, Pahang, Malaysia
[3]Faculty of Electrical and Electronic Engineering, Universiti Tun Hussein Onn Malaysia, Malaysia

ABSTRACT - Interbody fusion has recently been successfully used to treat degenerative spinal instability. Without needing to test it in vitro, finite element analysis (FEA) was used to reflect the biomechanical interaction between lumbars and cages. However, the complex geometry of the lumbar region was not accurately modeled by the numerous studies that relied on homogenous, simplified models. This study aims to fill this knowledge gap by creating an inhomogenous lumbar model and using computed tomography finite element analysis (CT-FEA) to assess the biomechanical characteristics of a spinal cage implanted in the model. CT images were used to create a 3D inhomogenous lumbar model of L4-L5. In order to assess the biomechanical characteristics of the implanted cage, a spinal cage was inserted between the lumbar model, and the model was subjected to FEA with loads ranging from 500 N to 1200 N. As the load applied to the assembled model varied from 500 N to 1200 N, the results showed that the maximum principal's stress increased. With values of 12.33 MPa and 0.102 Pa, respectively, the von Mises stress for a load of 500 N had the lowest maximum and minimum values. At 1200 N of force, the highest stress was indicated by the maximum and minimum values of the Von Mises Stress, which were 30.37 MPa and 0.244 Pa, respectively. The stress distribution demonstrated that the inhomogeneous lumbar model was applicable and that using FEA could produce promising results. The significance of taking into account the spinal cages' biomechanical characteristics in non-homogeneous lumbar models is shown by this study. CT-FEA can be a valuable tool for assessing the biomechanical characteristics of spinal cages in non-homogeneous lumbar models. The significance of taking into account the spinal cages' biomechanical characteristics in non-homogeneous lumbar models is shown by this study.

1.0 INTRODUCTION

Low back pain (LBP) is the main reason for activity restriction and job absence in many parts of the world. It is costly for individuals, families, communities, businesses, and governments. Several European studies have examined the social and economic effects of low back pain. With over 100 million lost workdays each year, low back pain was identified as the most prevalent disability among young adults in the United Kingdom [1]. Many causes of LBP have been discovered recently, including osteoarthritis, facet joint dysfunction, spondylolisthesis, compression fractures, and lumbar herniated discs[2].

Degeneration of intervertebral discs in the lumbar region of the spine can cause various spinal conditions that may require surgical intervention. One such intervention is using spinal cages made of various materials, such as titanium alloy, to support and stabilize the spine [3]. Finite Element Analysis (FEA) has been widely used to investigate the mechanical behavior of the lumbar region with spinal cages [4]. However, previous studies have some limitations.

The use of streamlined models that do not accurately depict the intricate geometry of the lumbar region is one of the limitations of earlier studies. Using linear or quasi-linear material models is another drawback because they might not accurately represent the nonlinear behavior of inhomogeneous materials [4]. Furthermore, the effects of various loadings on the mechanical behavior of the lumbar region with spinal cages have not been thoroughly investigated in earlier studies.

Furthermore, different loadings will be applied to the model to simulate various scenarios and investigate their effects on the mechanical behavior of the lumbar region. The effects of different load amounts on the model were studied by subjecting it to various uniformly distributed loads ranging from 500 N to 1200 N. The vertical total load applied represents the approximate body weight of a standing Asian male, which ranges from 50 kg to 120 kg.

This study uses FEA to examine the mechanical behavior of the lumbar region with a titanium alloy spinal cage. An accurate model of the lumbar region will be created for the study using detailed CT scan images, considering the intricate geometry of the intervertebral discs, vertebrae, and spinal cage. Nonlinear material models will be used to accurately represent the behavior of the titanium alloy material used in the spinal cage [5]. The results of this study will provide valuable insights into the mechanical behavior of the lumbar L4-L5 with a titanium alloy spinal cage and the effects of

different loadings on this behavior. With a titanium alloy spinal cage, the results of this investigation will shed important light on the mechanical behavior of the lumbar L4-L5 and the impact of various loadings on this behavior.

2.0   RELATED WORK

One of the treatments for a damaged disc that causes low back pain entails removing it and replacing it with a titanium cage filled with osteoconductive material or a bone graft extender made of hydroxyapatite between the two vertebrae. Titanium plates are attached to the vertebrae above and below the titanium cage with titanium pedicle screws to provide additional support for the spine after surgery. The purpose of the cage is to evenly distribute the loads placed on the spine until a solid biological fusion of the two lumbar regions, allowing for spine stability and ideal anatomic alignment. The fusion is essential because it prevents disc and motion segment degeneration if the motion of the adjacent segment is altered [6].

The 3D printed models in the medical industry can be used to improve CT scanning, which has aided pre-surgery planning and simulation of complex surgical or interventional procedures by providing a realistic replication of anatomy and pathology. The biomechanics of the human lumbar spine are commonly explained using finite element analysis (FEA) [7]. The biomechanical behavior of bones and soft tissues can also be predicted using FEA. In several pieces of literature, researchers have built distinct lumbar spine models for FEA. The vertebrae are interlocking bones that form a complex structure with intricate mechanical qualities to comprehend [4]. Using computed tomography (CT) scan images, a geometry-based L1-L5 lumbar spine model was built and validated using in-vitro experimental data. The CT scan was used to develop the lumbar spine model, which was then validated using experimental data [8]. Previous studies have attempted to develop and modify the FE model of the L1-L5 lumbar spine; to better understand the biomechanics of disc replacement and screw-based surgery [9]. A number of studies used the CT scan to generate an FE model of the L1–L5 lumbar spine to predict biomechanics after multilevel implantation [10]. In another study, a lumbar spine model was created to predict the optimal posture under various stress conditions such as compression, pure moment, and bending [11]. Overall, these studies highlight the need to understand better the lumbar spine's biomechanical behavior in various conditions.

A 3D model of a motorbike rider's lumbar spine bone (L-4) was created as part of a study by B. Jain, A. R. Tony, et al. (2020) to analyze biomechanical behavior during speed bumps. A CT scan of a healthy subject was used to create a three-dimensional (3D) FE model of the nonlinear L-4 lumber spine, which was then used to create the 3D model of the L4 lumbar. A three-dimensional (3D) geometry of the L-4 lumbar spine model was created by importing DICOM information from CT images. Then, 3D point cloud data was created using MIMICS software by importing two-dimensional (2D) CT scanning pictures. After that, segmentation and 3D building were possible thanks to the import of the 3D cloud data into SOLIDWORKS. A 3D reconstruction technique was used to accomplish surface smoothening. Figure 1 below displays the 3D L4 lumbar spine model created [12].
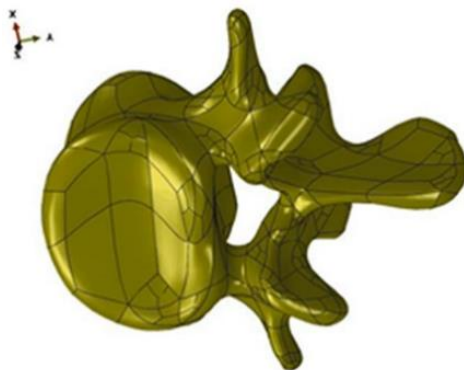

Figure 1. 3D model of Lumbar L4

FEA is a less expensive and more effective than in vivo and in vitro experimental tests. Internal biomechanical parameters of the bones and soft connective tissues in the spine can also be captured using FE modeling, which is difficult to measure using experimental methods. The material of osseous tissues of the vertebrae and cartilaginous endplates can be simulated as isotropic homogeneous linearly elastic materials in FEA software. Modifying other parts, such as the nucleus pulposus and annular ground materials, is possible. The number of elements in using FEA should be as high as possible. Therefore, mesh sensitivity analysis is applied to discover an acceptable mesh resolution with a large enough element number to assure simulation accuracy.

Some research was published on the mechanics of load transfer and stress distribution in the lumbar spine with rectangular cage-type interbody implants despite the increased usage of the spinal cage in the entire world [13]. C. Adam et al. conducted a study that showed a complete three-dimensional finite element simulation of the contact and internal stresses caused by compressive loading of rectangular cage-type implants against a vertebral body. According to the expert, finite element analysis of the vertebral endplate–implant construct will predict localized stresses for various implant and endplate characteristics.

The endplate subsidence loads at which endplate subsidence was most likely to happen were determined using the finite element model to forecast each component's stress, strain, and deformation levels under a specific compressive load. The stress levels for various material properties were then compared to those of the benchmark model using numerical sensitivity analyses. When the material parameters change, the patterns in output values provide a better understanding of the cage biomechanics in rectangular cage interbody implants [13]. The assembled model and its finite element mesh are shown in Figure 2.
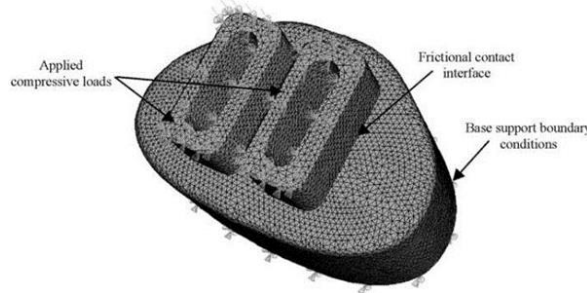

Figure 2. The assembled model and its finite element mesh

3.0 METHODOLOGY

3.1 Finite Element Modelling (FEM)

Figure 3 below shows the flow chart of this research to produce results from CT Scan to FEA. A flow chart for the CT-FEA of an inhomogeneous lumbar model and titanium alloy spinal cage model with different loadings depicted the steps involved in data acquisition, mesh generation, material properties definition, boundary conditions, solution, analysis, and reporting.
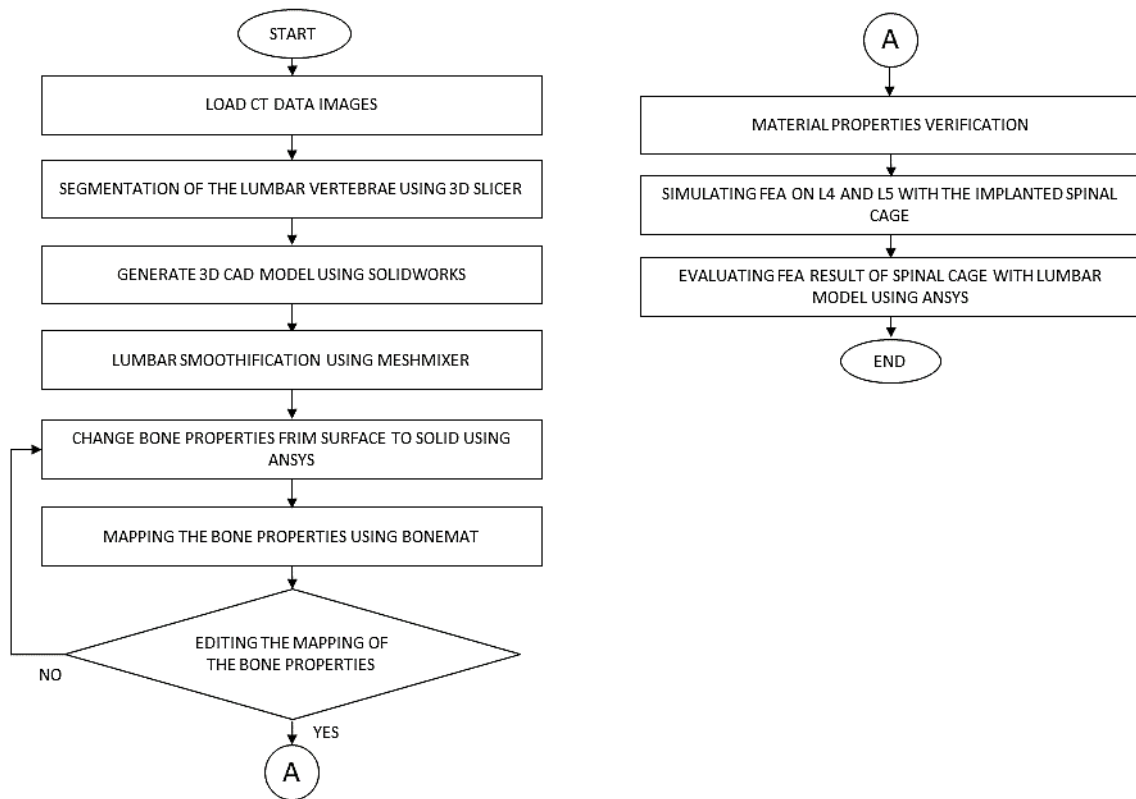

Figure 3. Flow chart

Using the CT images (Hitachi Activion16, Hitachi Medical Corporation, Tokyo, Japan) of a 29-year-old Japanese male patient without any lumbar spine-related musculoskeletal disease, distinct lumbar spine (L4-L5) finite element models were created. Prior to the research, the patient's written informed consent was obtained. [14] The DICOM data of the patient was put into the 3D Slicer software (3D Slicer, www.slicer.org) to make a 3D model [15]. This particular file is a DICOM data file, which holds the unprocessed data from a CT scan. The information is 512x512 pixels and pertains to CT modality with a slice thickness of 1.0 mm. There are 663 data points in all.

The DICOM files were loaded into the 3D Slicer software. Then, the volume definition and region segmentation were accomplished using the Volume rendering modules, as shown in Figure 4 below. The region of interest (ROI) was selected by trimming other parts, excluding the L4 and L5 vertebrae.
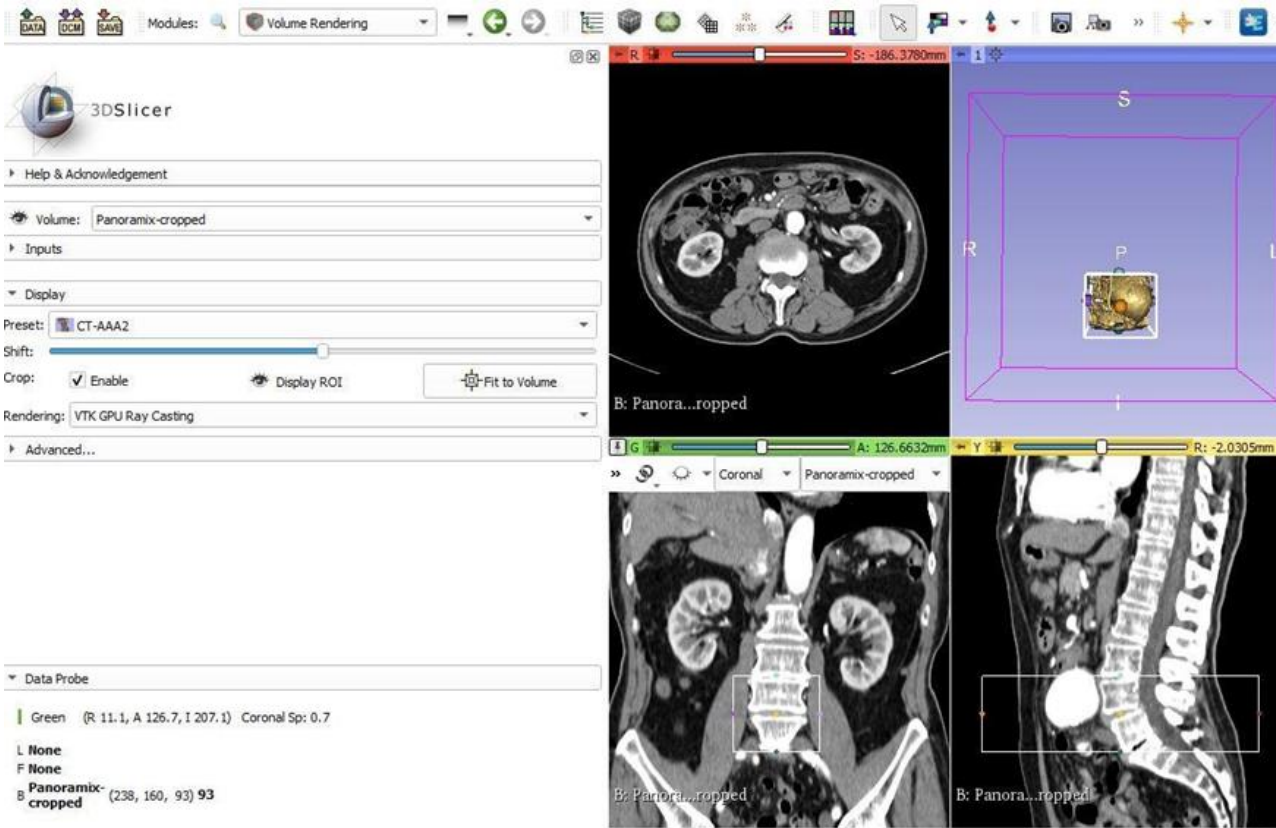

Figure 4. Selection of the region of interest (ROI) using volume rendering modules

The Segment Editor modules were then used to trim and modify the displayed ROI to remove extra bones and tissues. Figure 5 below shows the Segment Editor module used in this process.
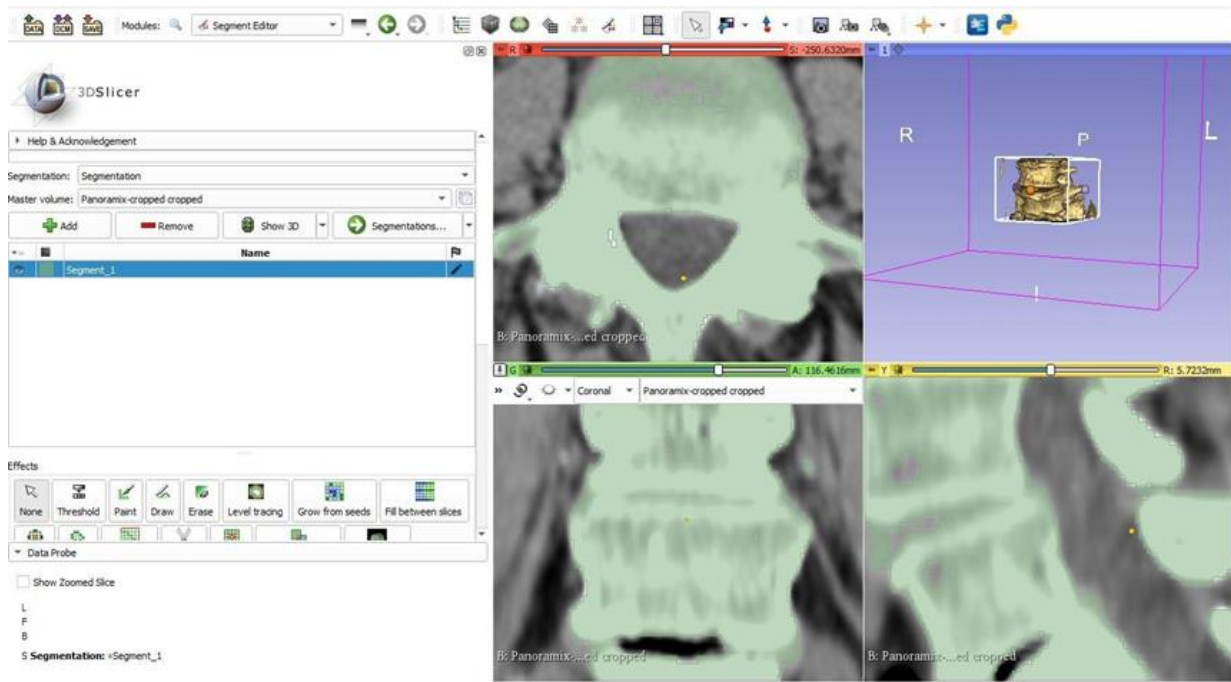

Figure 5. Segment editor module in 3D slicer

In order to facilitate more straightforward manipulation, the L4 and L5 were built as distinct 3D models. The region from the chosen threshold was combined using the Editor module. Figure 6 shows the finished L4-L5 model. The model was exported in STL format for the subsequent process involving the Meshmixer software (Autodesk Inc. San Rafael,

CA, USA). This application was used to correct the triangular vertebral mesh and smooth it out before sending the model to ANSYS (Ansys Inc., Canonsburg, PA, USA).
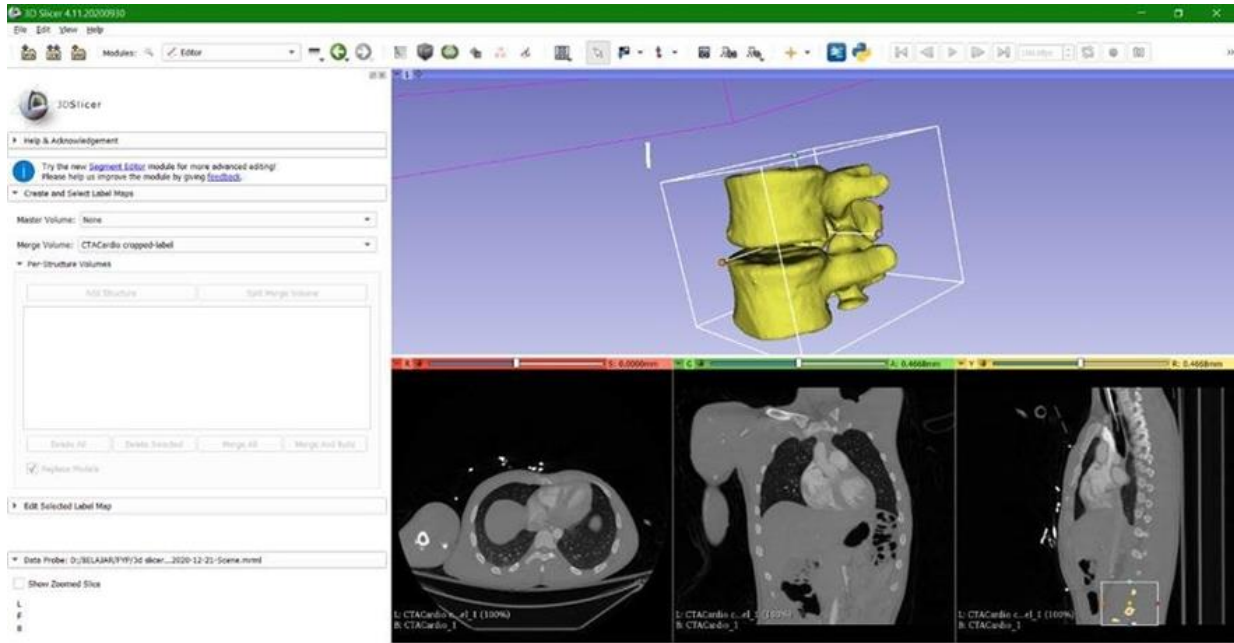

Figure 6. Editor module in 3D slicer

The surface mesh was then exported to the Bonemat software to translate the elastic bone characteristics generated from computed tomography images onto the Finite Element mesh.[16], [17] Using this software, the scalar field from a regular rectilinear CT image grid was mapped to the FE mesh model. The field of Hounsfield Unit (HU) numbers hosted by the CT images was transformed into a field of Young Modulus based on an algorithm parameter known as the HU integration [16], [18]. The configuration used for the HU integration in Bonemat is shown in the equation below.

$$\rho_{QCT} = -0.00393573 + 0.00791701(HU) \tag{1}$$

$$\rho_{ash} = 0.079 + 0.877\rho_{QCT} \tag{2}$$

$$E = 14664\rho_{ash}^{1.49} \tag{3}$$

Given the ash density, ρ_{ash} is in g·cm^{-3}, and Young Modulus, E is in GPa. A Poisson's ratio of 0.3 was used, while the HU numbers obtained from the rectilinear field of CT images are represented as the HU. The original solid model of the vertebrae was modified to include inhomogeneous element properties for each node, using Bonemat to divide the Young Modulus into three different intervals to define bone properties [19].

In this study, the Bonemat software was used to map the finite element mesh of the lumbar bone from CT images and assign elastic properties to each element. The HU integration was used to convert CT image intensity values to ρ_{ash} values, which were then used to determine the Young Modulus of the bone. The ash density measures the mineral content in the bone, which is directly related to the bone's stiffness. Therefore, by integrating HU values, we can estimate the ρ_{ash} and, in turn, determine the Young Modulus.

Some studies have suggested dividing the bone density range into multiple intervals to define the elastic properties more accurately. However, in this study, it was assumed that one interval would simplify the models and sufficiently capture the bone's mechanical behavior adequately. This assumption was made based on previous research and the availability of data [20]. The lumbar model's inhomogeneity was evaluated by observing the number of elements and their material properties. The mapped mesh model from Bonemat was exported to ANSYS again for FE analysis.

3.2   *Spinal cage design*

In this study, a design of the spinal cage model was chosen due to the significant characteristics shown by the specimen in the previous study [21]. The cage model was designed to be a patient-specific geometry by utilizing the height, width, and length of the intervertebral disc L4-L5. The design, namely, Specimen 2, was selected because it had the highest pore volume and low stress concentration compared to other design specimens. Both features were vital as they affect the bone grafting rate [21].

3.3   *Finite Element Analysis (FEA)*

ANSYS software was used to implant the spinal cage and lumbar model together. In order to simulate the posterior lumbar interbody fusion, the motion segments of the L4 and L5 models were subjected to a laminectomy and partial

discectomy. The posterior components, supraspinous, interspinous, ligamentum flavum ligaments, and partial disc were removed and replaced with a spinal cage and instrumentation system inserted in their spots. The spinal cage was oriented between the vertebral bodies within two-thirds of the disc space in the transverse plane. The model's orientation was significant in determining the position of the models inserted. [22][20].

The inferior surfaces of the L5 vertebral body were restricted in these models. The built model was loaded under various conditions, considering the patient's weight and typical daily activities.[23]. The model was evaluated with various uniformly distributed loads of 500 N, 600 N, 700 N, 800 N, 900 N, 1000 N, 1100 N, and 1200 N to study the effects of different loads exerted on the models. The value of the vertical total load applied represents the body weight of a standing Asian male, ranging from 50 kg to 120 kg.

The lumbar model and spinal cage were modified and combined using several software packages, including ANSYS Workbench, ANSYS Mechanical APDL, and SpaceClaim. Incorporating the titanium alloy spinal cage also adds to the complexity of the model and represents a realistic clinical scenario. The analysis of the different loadings applied to the model provides valuable information about the mechanical behavior of the lumbar region with spinal cages under various conditions.
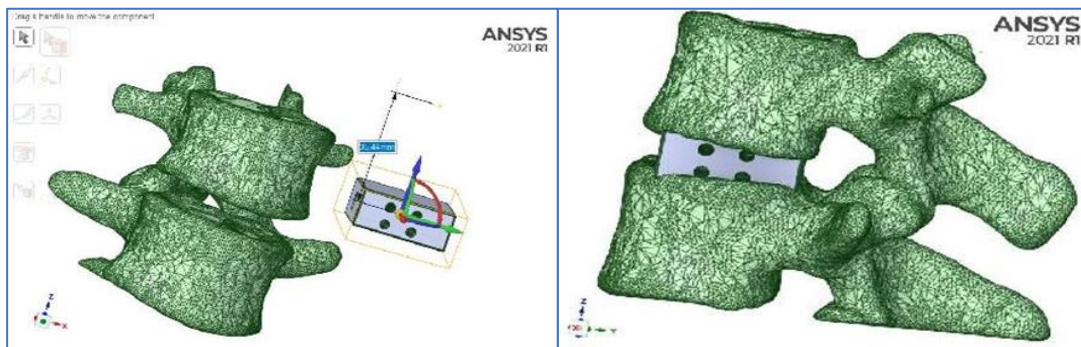

Figure 7. Assembling model of lumbar and spinal cage model

The SpaceClaim method to merge 3D lumbar data L4 and L5 is depicted in Figure 7. Before being tested in ANSYS Mechanical, the spinal cage must be in its exact location to ensure no errors. The portion of the cage and lumbar spine that intersected was eliminated using ANSYS' "Interference" function. This approach left the cage in its current state and simulated the interbody fusion procedure.

Various loads were applied to the superior surface of L4 for the simulation. At the same time, all nodes at the inferior surface of L5 were constrained in all degrees of freedom. The FEA simulation on the model is displayed in Figure 8 below.
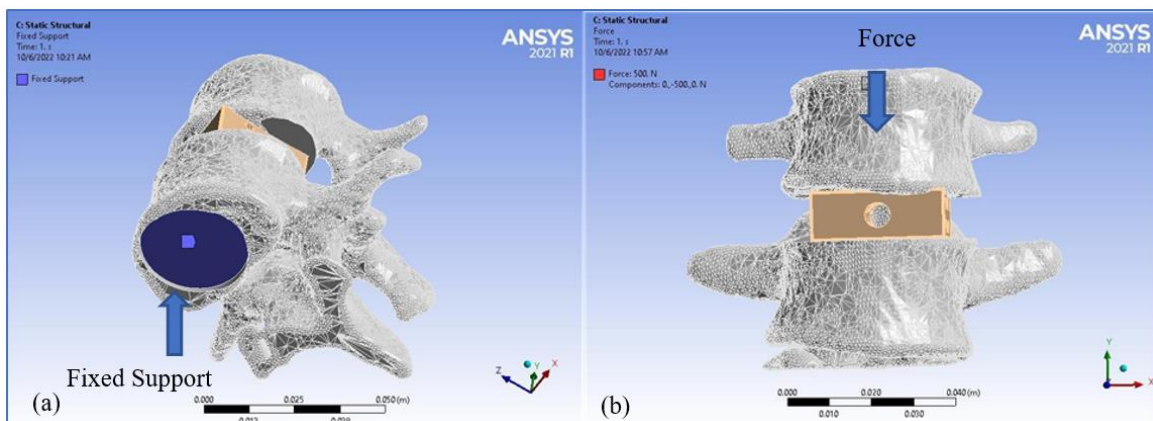

Figure 8. (a) Fixed support and (b) loading applied surface selection

4.0   RESULT AND DISCUSSION

4.1   *Inhomogeneous Lumbar Model*

The inhomogeneous lumbar model created using Bonemat software consists of 221818 elements with different Young Modulus values involved in developing the L4-L5 3D model. Using an inhomogeneous model is a significant improvement over previous studies that have used simplified models that do not accurately represent the lumbar region's complex geometry and material properties. The finite element analysis revealed that the mechanical properties of the inhomogeneous lumbar model varied greatly depending on the density of the vertebral body. The denser regions of the vertebral body showed increased stiffness and strength, while the less dense regions showed decreased stiffness and

strength. This study suggests that the inhomogeneous lumbar model accurately reflects the mechanical properties of the lumbar vertebrae in vivo.
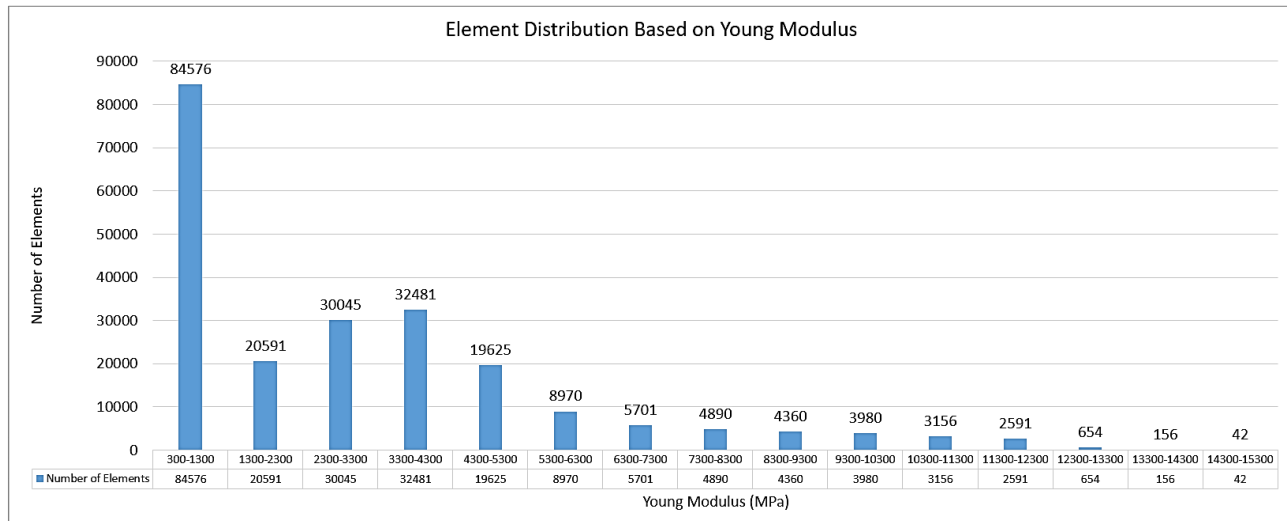

Figure 9. Histogram of element distribution

The maximum number of elements (84576) were plotted in the histogram at the Young Modulus range of 300 to 1300 MPa, according to Figure 9. These constituents comprise most of the cancellous bone region, which accounts for around 80% of the lumbar model and has a low modulus between 300 and 5300 MPa. The remaining 20% of the lumbar model comprises cortical bone.

4.2 Evaluation of Lumbar Model Geometry

The outcome of the 3D Lumbar L4 and L5 model created with ANSYS software is shown in Figure 10 below. The 3D lumbar model, which depicts its numerous components, displays various hues, demonstrating the success of the inhomogeneous procedure. Furthermore, due to the production method's ability to precisely match the size and shape, this model's shape closely resembles an actual lumbar. As a result, creating a spinal cage using this approach can significantly lower the possibility of negative consequences and be customized to the patient's unique lumbar size.
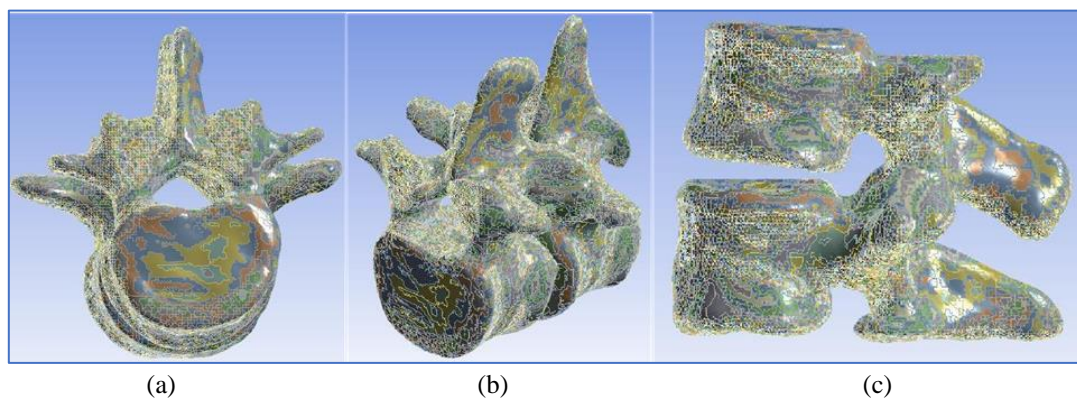

      (a)   (b)   (c)

Figure 10. (a) Top, (b) isometric, and (c) side view of model lumbar developed

The current lumbar model was evaluated compared to the one presented in a previous study, highlighting the shared similarities in their foundational anatomical representations. The created lumbar model, shown in Figure 11(a), was comparable to the previous study, which used the same raw data with ROI of L3-L4 [24]. However, because of the limitations of the initial CT images, the spinous process of lumbar L5 (the lower part of L5) demonstrated a considerable defect at the proximity of L5 facet joints. However, this discrepancy could be overlooked because the entire surface of the lower part of the lumbar L5 will be limited (configured as a fixed support). The lumbar model was thus appropriate for use in simulation and analysis.
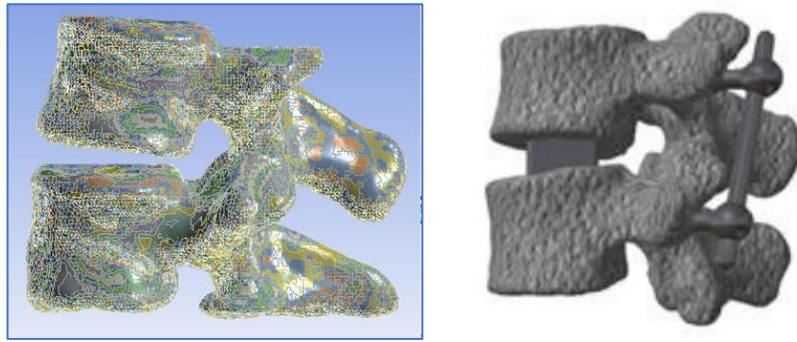
Figure 11. (a) Compare the Developed L4-L5 Model with (b) the previous study of L3-L4

4.3   FEA Result

The simulations of the inhomogeneous lumbar with different loads in the spinal cage have successfully produced results drawn in graph form to facilitate understanding. This graph contains the von Mises stress against the applied force. Von Mises stress is a commonly used variant stress metric that considers all standard and shear stress components acting on a single point in the material. Critical von Mises stress values for ductile materials are frequently used to define the onset of failure [25]. The uneven stress distribution beneath each implant's contacting faces is a critical observation that carries significant implications for the structural integrity and performance of the implants. This non-uniform stress distribution is relevant since it directly affects the implant system's long-term durability, safety, and operation.
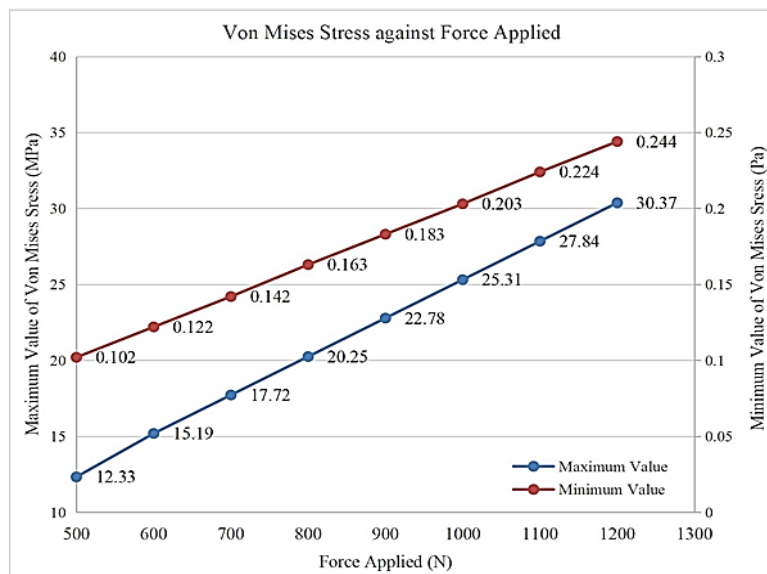

Figure 12. Von Mises Stress against Force Applied

Figure 12 shows that the amount of force applied on the surface of the lumbar was directly proportional to the maximum value of Von Mises Stress. From the figure above, the stress of load 500N had the lowest value for both maximum and minimum, with 12.33 MPa and 0.102 Pa, respectively. Meanwhile, when the highest force applied was 1200 N, the maximum and minimum values of Von Mises Stress showed the highest stress with 30.37 MPa and 0.244 Pa, respectively.
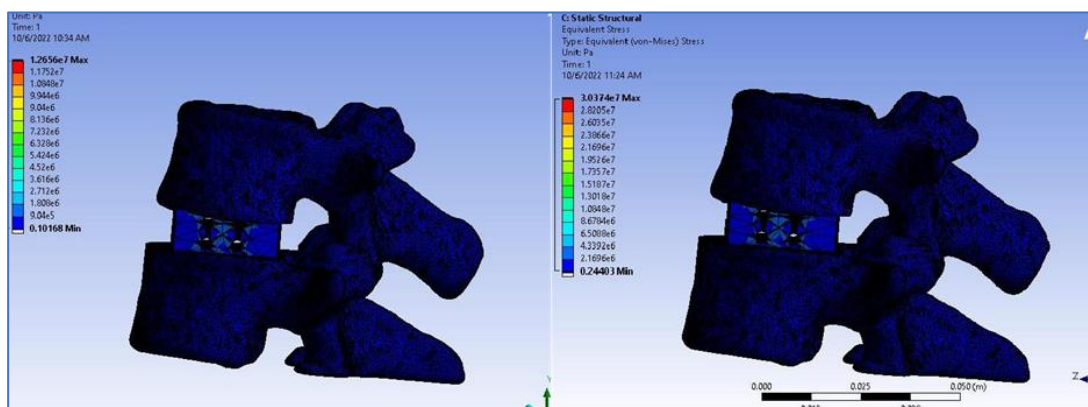

Figure 13. Von Mises Stress of 500 N and 1200N Load Applied

Figure 13 above shows the equivalent stress (Von Mises Stress) when 500 N was exerted on the assembled model. From the figure, the maximum value of Von Mises Stress was 12.656 MPa, and the minimum value of Von Mises Stress was 0.1017 Pa. It was figured that the maximum stress of 12.656 MPa occurred at the hole of the spinal cage. Meanwhile, at the spinal cage, when the vertical load was applied on the surface of lumbar L4, the stress contour on the lumbar model was concentrated more on the region that was in contact with the surface of the spinal cage. The stress concentration region was identical for all the loads applied.

The maximum and minimum values of Von Mises Stress when 1200 N load was applied were 30.37 MPa and 0.244 Pa, respectively, as shown in the figure above. Both minimum and maximum stress values obtained with a 1200 N load applied are probably the highest since this study had the highest load applied. The figures of the stress simulation result above showed the predicted von Mises stresses in the assembled model. The maximum value of Von Mises Stress for the models ranges from 12.656 MPa to 30.374 MPa.

The high-stress locations in the implant (anterior and posterior edges) correspond to the high-stress locations on the adjacent vertebral endplate, as shown in Figure 14 below.
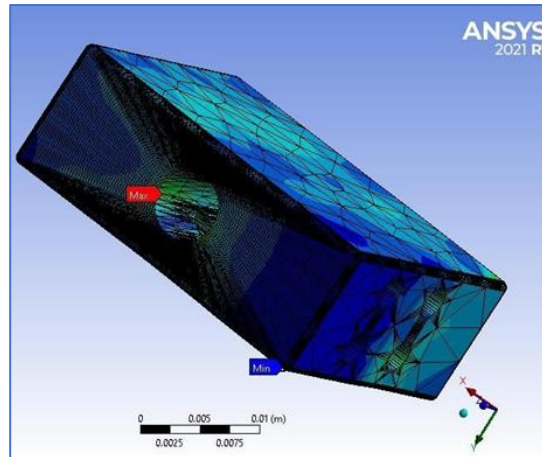

Figure 14. Stress location on spinal cage

Based on the colored contours of stress distributed during the simulation, it was shown that most of the stress occurred at the cage's holes. The discontinuity in the structure directly caused this part to be the primary region to experience the highest stress concentration. The stress also concentrated on the contacted surface of the lumbar and spinal cage model. This stress result was the same for all the loads applied (500 N to 1200 N) in this analysis. Although maximum everyday stress in the contact region will be the same for an implant and vertebral endplate, the magnitude of Von Mises (or principal stresses) within each body adjacent to the contact region differs due to the different geometry of each component.

The principal stress levels in the cancellous core were predicted to be much lower than those in the cortical shell. These lower stress levels were due firstly to the low elastic modulus of cancellous bone compared to cortical bone. Secondly, the direct compressive load application that the cancellous core experiences, as opposed to the indirectly induced bending loads in the cortical shell. The cancellous core was essential in supporting the vertebral endplate under compressive loading.

The analysis of Maximum Principal Stress shows positive and negative stress data for this simulation. It represents the tensile and compressive principal stresses on the model. It can be seen in Figure 15 that the linear-like relationship of Maximum Principal Stress against Force Applied. However, the slope was different for maximum and minimum values of stress. The maximum values of stresses obtained from the models were the tensile stress present during the simulation, while the minimum values of stresses represent the compression stress that occur. Both the maximum and minimum lines show an increasing value when more force is applied to the model. The maximum principal's stress increased as the load applied on the assembled model varied from 500 N to 1200 N, and the range of principal (tensile) and (compression) stress also increased from 5.045 MPa to 12.108 MPa and 6.779 MPa to 16.27 MPa, respectively.
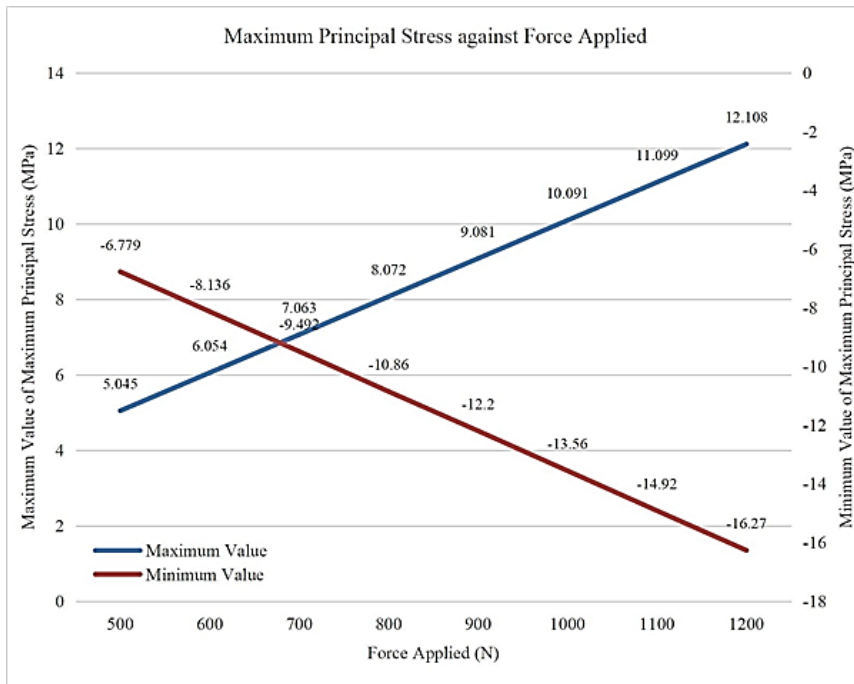
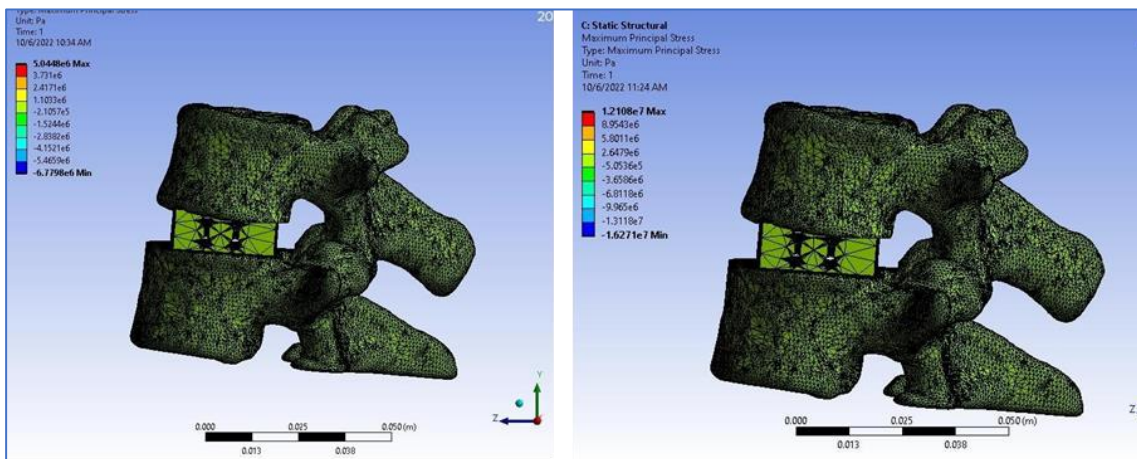Figure 15. Maximum Principal Stress against Force Applied

Figure 16. Maximum Principal Stress of 500N and 1200N Applied Load

From Figure 16 above, when a 500 N load was applied, the model shows a minor stress concentration compared to other load amounts exerted. This load's maximum and minimum principal stress values are 5.045 MPa and -6.78 MPa, respectively. The amount of tensile stress of 5.045 MPa and 6.78 MPa of compression stress is executed.

The model in the figure also seems to exert high stress due to the high load applied. The force applied of 1200 N caused the middle surface region (the contacted region of the lumbar and cage) to favor having the highest stress concentration of 12.108 MPa of maximum value and -16.271 MPa of minimum value of Maximum Principal Stress.

5.0   CONCLUSIONS

Incorporating inhomogeneous lumbar models with spinal cages made of titanium alloy and analyzed under eight different loading conditions presented a favorable method for managing spinal disorders. The study, which employed DICOM data from raw CT images, utilized 3D Slicer software to transform the DICOM data to STL, employed Meshmixer to correct mesh issues, utilized Bonemat software to convert bone properties into inhomogeneous properties, and used ANSYS to simulate the FEA. The outcomes of this study establish the viability of this technique and its capacity to enhance spinal stability while minimizing the probability of implant malfunction. The model of the lumbar spine and the spinal cage were successfully assembled in this study, and FEA simulations were conducted. Overall, this research highlights the importance of combining advanced imaging techniques and computational modeling to improve our understanding of spinal biomechanics and the performance of spinal implants. The findings of this study may inform the development of novel spinal implant designs and advance the field of spinal surgery, ultimately leading to better outcomes for patients with spinal disorders. Future studies with larger sample sizes and more accurate material properties are needed

to further understand the lumbar region's mechanical behavior under varying conditions. The study highlights the need to consider segmenting L4 and L5 separately using the sectioning feature in ANSYS. So, the study on stress distribution on each lumbar can be analyzed in detail to analyze the graph of stress distribution at the lumbar endplate. The results of the finite element analysis suggest endplate stresses and potential for compressive subsidence failure could be reduced with conforming endplate and implant surface profiles, with particular attention to the outer edges of the implant (closer to the periphery of the endplate) for a given transmitted load.

6.0   CONFLICT OF INTEREST

We have no conflicts of interest to disclose. All authors declare that they have no conflicts of interest.

7.0   ACKNOWLEDGEMENT

8.0   REFERENCES

[1]   C. E. Lavecchia, D. M. Espino, K. M. Moerman, K. M. Tse, D. Robinson, P. V. S. Lee, and D. E. T. Shepherd, "Lumbar model generator: A tool for the automated generation of a parametric scalable model of the lumbar spine," *Journal of The Royal Society Interface*, vol. 15, no. 138, 2018.

[2]   N. N. Knezevic, K. D. Candido, J. W. S. Vlaeyen, J. Van Zundert, and S. P. Cohen, "Low back pain," *Lancet*, vol. 398, no. 10294, pp. 78–92, 2021.

[3]   R. Gunzburg, C. J. Colloca, C. F. Jones, D. J. Hall, J. McAviney, S. Callary, M. A. Hegazy, M. Szpalski, and B. J.C. Freeman, "Does nanoscale porous titanium coating increase lumbar spinal stiffness of an interbody fusion cage? An in vivo biomechanical analysis in an ovine model," *Clinical Biomechanics*, vol. 67, no. July, pp. 187-196, 2019.

[4]   Z. Zhang, H. Li, G. R. Fogel, Z. Liao, Y. Li, and W. Liu, "Biomechanical analysis of porous additive manufactured cages for lateral lumbar interbody fusion: A finite element analysis," *World Neurosurgery*, vol. 111, no. March, pp. e581-e591, 2018.

[5]   J. J. Liou and and T. I. El-Wardany, "Finite element analysis of residual stress in Ti-6Al-4V alloy plate induced by deep rolling process under complex roller path," *International Journal of Manufacturing Engineering*, vol. 2014, no. 1, pp. 1-14, 2014.

[6]   T. L. T. Siu, E. Najafi, and K. Lin, "Lateral lumbar interbody fusion at L4-5: A morphometric analysis of Psoas anatomy and cage placement," *World Neurosurgery*, vol. 141, pp. e691–e699, 2020.

[7]   V. K. Meena, P. Kalra, and R. K. Sinha, "Finite element study on the influence of pore size and structure on stress shielding effect of additive manufactured spinal cage," *Computer Methods in Biomechanics and Biomedical Engineering,* vol. 25, no. 3, pp. 566–577, 2022.

[8]   J. Berger-Groch, D. M. Thiesen, F. Ntalos, F. Hennes, and M. J. Hartel, "Assessment of bone quality at the lumbar and sacral spine using CT scans: a retrospective feasibility study in 50 comparing CT and DXA data," *European Spine Journal*, vol. 29, no. 5, pp. 1098–1104, 2020.

[9]   M. Macki, T. Hamilton, Y. W. Haddad, and V. Chang, "Expandable Cage Technology - Transforaminal, Anterior, and Lateral Lumbar Interbody Fusion," *Oper. Neurosurg*, vol. 21, no. Suppl 1, pp. S69–S80, 2021.

[10]   P. Tahvonen, H. Oikarinen, and O. Tervonen, "The effect of interventions on appropriate use of lumbar spine radiograph and CT examinations in young adults and children: a three-year follow-up," *Acta Radiologica: Sage Journals,* vol. 61, no. 8, pp. 1042–1049, 2020.

[11]   Z. Zhang, H. Li, G. R. Fogel, D. Xiang, Z. Liao, and W. Liu, "Finite element model predicts the biomechanical performance of transforaminal lumbar interbody fusion with various porous additive manufactured cages," *Computers in Biology and Medicine*, vol. 95, no. February, pp. 167–174, 2018.

[12]   B. Jain A R Tony, M. S. Alphin, and G. Sri Krishnan, "Simulation of L-4 lumbar spine model of motorist exposed to vibration from speed hump," *Journal of Orthopaedics*, vol. 22, pp. 390–396, 2020.

[13]   M. Zhang *et al.*, "Development of an integrated CAD–FEA system for patient-specific design of spinal cages," *Computer Methods in Biomechanics and Biomedical Engineering*, vol, 20, no. 4, pp. 1-10, 2016.

[14]   M. H. Jalil, M. H. Mazlan, and M. Todo, "Biomechanical Comparison of Polymeric Spinal Cages Using Ct Based Finite Element Method," *International Journal of Bioscience, Biochemistry and Bioinformatics*, vol. 7, no. 2, pp. 110–117, 2017.

[15]   A. Fedorov *et al.*, "3D Slicer as an image computing platform for the quantitative imaging network," *Magnetic Resonance Imaging,* vol. 30, no. 9, pp. 1323–1341.

[16]   F. Taddei, E. Schileo, B. Helgason, L. Cristofolini, and M. Viceconti, "The material mapping strategy influences the accuracy of CT-based finite element models of bones: An evaluation against experimental measurements," *Medical Engineering & Physics*, vol. 29, no. 9, pp. 973–979, 2007.

[17]   E. Schileo, J. Pitocchi, C. Falcinelli, and F. Taddei, "Cortical bone mapping improves finite element strain prediction accuracy at the proximal femur," *Bone*, vol. 136, p. 115348, Jul. 2020.

[18]   M. Viceconti, M. Qasim, P. Bhattacharya, and X. Li, "Correction to: Are CT-Based Finite Element Model Predictions of Femoral Bone Strength Clinically Useful?" *Current Osteoporosis Reports*, vol. 16, pp. 216–223, 2018.

[19]   J. H. Keyak, "Improved prediction of proximal femoral fracture load using nonlinear finite element models.," *Medical Engineering & Physics*, vol. 23, no. 3, pp. 165–73, 2001.

[20]   M. H. Jalil, M. H. Mazlan, and M. Todo, "Validation of Compressive Test of Biodegradable Lumbar Interbody Spinal Cage with Different Porous Structure Using Computed Tomography-Based Finite Element Analysis," in *Lecture Notes in Mechanical Engineering; Human-Centered Technology for a Better Tomorrow*, pp. 153–167, 2022.

[21]   K. Mahendran and M. H. Jalil, "Finite element analysis of different spinal cage designs for posterior lumbar interbody fusion," in *Proceedings of International Exchange and Innovation Conference on Engineering & Sciences (IEICES)*, 2021, vol. 7, pp. 51–57.

[22]   M. H. Mazlan, M. Todo, H. Takano, and I. Yonezawa, "Effect of Cage Insertion Orientation on Stress Profiles and Subsidence Phenomenon in Posterior Lumbar Interbody Fusion," *Journal of Medical and Biological Engineering*, vol. 5, no. 2, pp. 1–6, 2016.

[23]   P. I. Tsai, C. C. Hsu, S. Y. Chen, T. H. Wu, and C. C. Huang, "Biomechanical investigation into the structural design of porous additive manufactured cages using numerical and experimental approaches," *Comput. Biol. Med.*, vol. 76, no. September, pp. 14-23, 2016.

[24]   R. Yahya, M. H. Mazlan, S. Shuib, and A. H. Abdullah, "Biomechanical Analysis of Spinal Fusion Cage for Lumbar Vertebrae," *International Journal of Recent Technology and Engineering*, vol. 8, no. 4, pp. 6859–6863, 2019.

[25]   Y. H. Tsuang, Y. F. Chiang, C. Y. Hung, H. W. Wei, C. H. Huang, and C. K. Cheng, "Comparison of cage application modality in posterior lumbar interbody fusion with posterior instrumentation-A finite element study," *Medical Engineering & Physics*, vol. 31, no. 5, pp. 565–570, 2009.